



Research Article

Experimental and numerical analysis of ceramic fiber geopolymer concrete under blast effect

Aras Dalğıç ¹, Berivan Yılmaz Polat ², *, Sedat Savaş ³

¹ Department of Civil Engineering, Munzur University, Tunceli (Turkey); adalgic@firat.edu.tr

² Department of Architecture, Munzur University, Tunceli (Turkey); bpolat@munzur.edu.tr

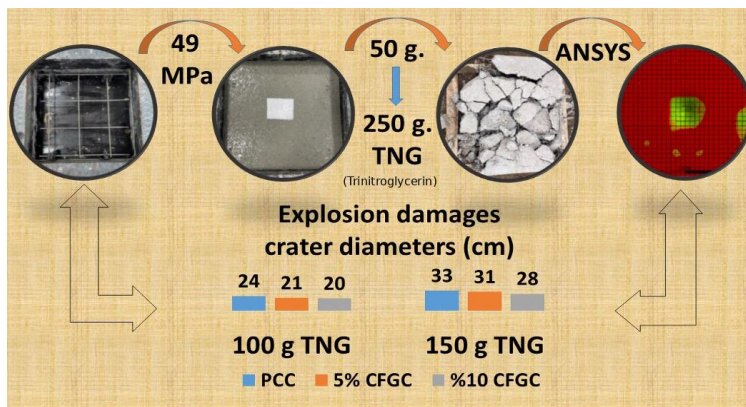
³ Department of Civil Engineering, Firat University, Elazığ (Turkey); ssavas@firat.edu.tr

*Correspondence: bpolat@munzur.edu.tr

Received: 08.09.24; Accepted: 05.02.26; Published: 06.03.26

Citation: Dalğıç, A., Yılmaz Polat, B. and Savaş, S. (2026). Experimental and numerical analysis of ceramic fiber geopolymer concrete under blast effect. *Revista de la Construcción. Journal of Construction*, 25(1), 110-128. <https://doi.org/10.7764/RDLC.25.1.110>

Graphical abstract:



Highlights:

- 10% GFCC showed less crack formation and lower shrapnel effect compared to PCC.
- The addition of ceramic fibers increased the blast resistance of geopolymer concrete.
- CFGFC is more resistant to high temperatures and high pressures compared to PCC.
- Fast and cost-effective predictions were made in concrete designs using ANSYS-Workbench.
- The results highlight the advantages of using CFGFC in future engineering projects.

Abstract: This study employs both experimental and numerical methods to investigate the blast resistance of ceramic fiber-reinforced geopolymer concrete (CFGFC), a cement-free material often referred to as green concrete due to its environmentally friendly nature compared to Portland cement concrete (PCC). Geopolymer concrete specimens, formulated with ground granulated blast furnace slag, silica fume, and varying proportions of ceramic fibers, were subjected to blast tests using 50, 100, 150, 200, and 250 grams of trinitroglycerin (TNG). A standard PCC specimen was utilized as a control. The results demonstrate that the incorporation of 10% ceramic fibers significantly enhances the blast resistance of the geopolymer concrete, reducing crater diameters by up to 20% compared to conventional PCC. Furthermore, the finite

element model developed in ANSYS Workbench exhibits a strong correlation with the experimental data, validating the predictive capability of the numerical simulations. Overall, this research highlights the immense potential of CFGC as a sustainable, highly durable alternative for structures exposed to blast loads.

Keywords: Geopolymer concrete, ceramic fiber, blast tests, finite element method, ground granulated blast furnace slag, silica fume.

Abbreviation:

PCC: Portland cement concrete

CFGC: Ceramic fiber reinforced geopolymer concrete

5% CFGC: 5% ceramic fiber reinforced geopolymer concrete

10% CFGC: 10% ceramic fiber reinforced geopolymer concrete

TNT: Trinitrotoluene

TNG: Trinitroglycerin

Na₂SiO₃: Sodium silicate

NaOH: Sodium hydroxide

CaO: Calcium oxide

SiO₂: Silicon dioxide

Al₂O₃: Aluminum oxide

FEM: Finite element method

1. Introduction

Whether accidental or intentional, explosions pose serious threats to critical infrastructure and often lead to devastating loss of life and property. These losses are further amplified by the disintegration and spalling of conventional concrete structures caused by the explosion, producing deadly shrapnel fragments. While Portland cement concrete (PCC) remains the most widely used construction material globally due to its ease of application, high compressive strength, and durability, its production releases significant amounts of carbon dioxide (CO₂) into the atmosphere, posing a major environmental problem (Hardjito and Rangan, 2005; McCaffrey, 2002; Naik, 2008; V. M. Malhotra, 2002; Vora and Dave, 2013). Consequently, there is a significant need to develop alternative materials in the construction sector that reduce the carbon footprint while exhibiting high structural performance under extreme dynamic loads. In this context, investigating the explosion response of geopolymer concrete is of paramount importance.

On the other hand, to understand the response of both conventional PCC and geopolymer concretes to blast loading, it is necessary to know the properties of explosives. In civil engineering and defense applications, concentrated high explosives (such as solid or liquid charges) are a primary concern due to their enormous energy densities and rapid detonation velocities. When these explosives detonate, they generate a highly destructive shock wave with local peak temperatures ranging from 3000 to 4000 °C and blast pressures reaching up to 30 GPa very rapidly. When this highly destructive shock

wave interacts with a concrete element, it creates large compressive and tensile stress waves, leading to severe local damage and fragmentation (Agrawal, 2010; Duc Ngo, Tuan; Mendis, P.;Gupta, A.;Ramsay, 2007; Mortar et al., 2017). The high temperature and high pressure values after the explosion can cause severe damage to concrete. In their study, Shi et al. investigated the component properties and local damage mechanism of reinforced concrete slabs under close proximity blasts. In that study, five concrete slabs were tested under different blast loads generated by 2 kg, 4 kg and 6 kg trinitrotoluene (TNT) charges, respectively. The distance between the explosives and the specimens was 0.4 m. Comparing the damage zones of the five specimens, it was found that localized damage such as fragmentation and crushing was more likely to occur under close-range blasts. Using 6 kg TNT, the maximum ejection velocity of fragments from concrete slabs under close-range blast loads was found to be up to 100 m/s. In the study, it was concluded that concrete fragments with high ejection velocity will cause serious damage to the environment (Shi, Wang, and Cui, 2020).

In previous studies, fiber reinforcement was generally applied to geopolymer concretes to reduce the damage caused by explosions. Meng et al. investigated the behavior of steel fiber-reinforced geopolymer concrete panels against blast loading. In that study, they observed that steel fiber-reinforced geopolymer concrete panels dissipated the blast energy more uniformly (Meng et al., 2019a). In another study, Meng et al. investigated methane gas explosions (flaring) in buried utility tunnels. They designed the buried service tunnel with steel fiber-reinforced geopolymer concrete composite (Meng et al., 2020). Steel fiber-reinforced geopolymer concretes were tested with 50 kg TNT placed at different distances. In that study, steel rebar-reinforced C30 concrete slabs were produced for comparison with geopolymer concrete specimens. For the explosive placed at 3 meters distance, both C30 concrete slab and steel fiber reinforced geopolymer concrete slab did not give positive results. However, geopolymer specimens showed less crack formation than C30 concrete specimens in the blast tests performed at 5 meters and 7 meters. The post-blast results showed that geopolymer concrete has good compressive and flexural strength under static load.

In addition, the compressive strength of plain geopolymer concrete was 61 MPa, while the compressive strength of steel fiber-reinforced geopolymer concrete was 74 MPa (Meng et al., 2020). Meng et al. researched the behavior of geopolymer concrete slabs formed using blast furnace slag and silica fume under blast loading. In that study, steel rebar-reinforced C30 concrete slabs were produced as control specimens. Geopolymer and control specimens were positioned at 3, 5 and 7 m distances. All specimens were subjected under 200 kg TNT. As a result of the study, it was observed that the geopolymer specimens were less damaged than the control specimens (Meng et al., 2019b). Polat et al. explored the damaging effect of explosives such as rocket warheads and TNT on concrete slabs with different geometries. As a result of this study, it was determined that the damage mode decreased by leaving voids in the internal structure of concrete slabs (Polat, Savaş, and Polat, 2023). Wu et al. numerically investigated the structural dynamic response and collapse behavior of reinforced concrete slabs subjected to TNT blasts under different conditions. They modelled the results by blasting concrete slabs with dimensions of 100x100x40 cm with the help of TNT positioned at 40 cm. The TNT weights used in this study were 0.20, 0.31, 0.46, 0.55 kg (Wu et al., 2020).

Li et al. exposed composite concrete material with construction steel and extra steel mesh reinforcement to a 1 kg TNT blast in their study. They compared the blast responses of the specimens using steel mesh reinforcement at 2%, 4% and 6% by volume. In that study, modeling was performed using coupled finite elements and smoothed particle hydrodynamics (Li, Wu, Hao, and Su, 2017). Foglar et al. compared the numerical and experimental results of concrete slabs with different compressive strengths produced using waste steel and polypropylene fibers under TNT blasts (Foglar, Hajek, Kovar, and Štoller, 2015). In their study, Nili et al. compared the impact strength of steel fiber-reinforced concrete with and without silica fume addition. As a result of the study, impact resistance and ductility were higher in concrete prepared using silica fume and steel fiber (Nili and Afroughsabet, 2010).

Ma et al. investigated the mechanical properties of ceramic fiber reinforced Portland cement composites. As a result of this study, they found that the flexural strength of the specimens with ceramic fiber added increased significantly (Ma, Zhu, and Tan, 2005a). Haruna et al. subjected polyurethane-based polymer concrete to repeated weight drop impact test to investigate its impact resistance properties. Normal concrete specimens were tested for comparison. As a result, it shows that the polyurethane binder composition greatly increases impact times and energy absorption capacity (Ibrahim Haruna, Zhu, Jiang,

and Shao, 2021). Yazici et al. investigated the mechanical properties of steel fiber concrete subjected to impact loading. In their study, they used three different steel fibers with aspect ratios of 45, 65 and 80 at 0.5%, 1.0% and 1.5% by volume, respectively. The compressive strength of these steel fiber-concrete mixtures was found to be approximately 50 MPa. Concrete specimens without fibers were used as control specimens. The prepared specimens were subjected to impact tests by drop-weight and the impact fracture energies were determined. As a result of this study, the loss of mechanical properties in concretes with steel fibers subjected to impact loads was significantly reduced compared to concretes without fibers. Steel fibers reduced the rupture effect of the impact on the concrete by absorbing part of the impact and distributing the impact throughout the specimen (Yazici, Arel, and Tabak, 2013).

Dalğıç and Polat investigated the behavior of geopolymer concrete specimens with different ratios of ceramic fibers added and PCC specimens without fiber reinforcement against high temperatures and found that the specimens with high ceramic fiber ratio showed significantly less damage mode when exposed to high temperatures (Dalğıç and Yılmaz Polat, 2024). Ma Yiping et al. investigated the mechanical properties of cementitious composites with ceramic fiber addition. It was found that the addition of ceramic fiber to the cement mortar at 5% by volume increased the flexural strength by about 40%. It was also found that when silica fume was added to this mortar to reduce the particle size of the matrix, the flexural strength could increase up to 100% (Ma, Zhu, and Tan, 2005b). Su et al. investigated the mechanical properties of ceramic fiber reinforced concrete under dynamic and static pressure. They found that properties such as strength, energy absorption and critical stress increased significantly with the addition of ceramic fibers to concrete (Su, Xu, and Ren, 2014).

While several studies have investigated the mechanical properties of ceramic fiber-reinforced structures, existing research has predominantly utilized ceramic components as external or internal coatings in solid forms, such as foams or panels. However, the potential of ceramic fibers to interact with the geopolymer matrix to form a more homogeneous, gel-like structure—and how this prospective microstructural transformation contributes to the explosive spalling resistance of concrete at elevated temperatures—remains insufficiently explored. This paper aims to bridge this research gap by investigating the effects of ceramic fiber incorporation on the mechanical properties and explosive spalling behavior of geopolymer concrete, employing both experimental and advanced numerical modeling approaches. The remainder of this paper is structured as follows: Section 2 details the experimental program and materials; Section 3 discusses the experimental and numerical findings; Section 4 summarizes the main conclusions of the study; and Section 5 outlines the implications for structural design applications.

2. Materials and methods

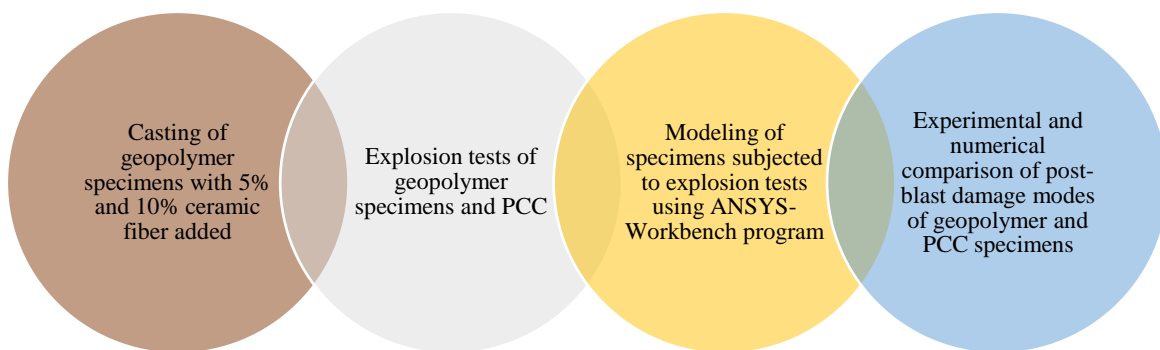


Figure 1. Flow chart of the study.

In this study, ground granulated blast furnace slag, silica fume, ceramic fibers, superplasticizer, sodium silicate (Na_2SiO_3), sodium hydroxide (NaOH), fine aggregate, and coarse aggregate were used to produce geopolymer concrete. The ground blast furnace slag used in the study contains 33% calcium oxide (CaO), while the silica fume contains approximately 1.06-1.80% CaO by mass. The alkaline liquids NaOH and Na_2SiO_3 were supplied by Tekkim and are of analytical purity. Furthermore, the NaOH concentration used in the study is 12 M. The melting point of the ceramic fibers used in the concrete is 1760 °C.

The diameter of the fibers varies between 2.6 μm and 3.4 μm , and their chemical composition consists of 52% silicon dioxide (SiO_2) and 44% aluminum oxide (Al_2O_3).

Within the scope of this study, ceramic fiber-reinforced geopolymer concrete (CFGC) specimens and a Portland cement concrete (PCC) control specimen were tested. The PCC was produced using CEM II 52.5 cement. Compressive strength was measured after the prepared PCC specimens were cured under laboratory conditions for 28 days. The average compressive strength of the PCC at 28 days was found to be 49 MPa. The geopolymer concrete contained 90% ground granulated blast furnace slag and 10% silica fume as a binder. Based on the laboratory trials, geopolymer concrete was prepared with the proportions detailed in Table 1 and yielded an average compressive strength of 50 MPa at 28 days. Furthermore, the incorporation of ceramic fibers in this mix design was motivated by a recent study (Dalğıç and Yılmaz Polat, 2024), which demonstrated that geopolymer concrete with high ceramic fiber ratios exhibits significantly reduced damage when exposed to elevated temperatures.

Table 1. Geopolymer concrete mixing ratios (kg/m^3).

Fine agg.	Coarse agg.	Binders		Activators		Superplasticizer
		Silica fume	Slag	Na_2SiO_3	NaOH	
1209	651	40	360	115	46	4

Test specimens measuring $50 \times 50 \times 10$ cm were prepared for the blast tests. A total of 15 specimens were cast, comprising three groups: five specimens of 5% ceramic fiber-reinforced geopolymer concrete (5% CFGC), five specimens of 10% CFGC, and five PCC control specimens (which contained no ceramic fibers). In all specimens, a Q131/131 type steel mesh (5 mm diameter with 15 cm spacing) was placed at the mid-depth of the concrete cross-section. The casting molds and the arrangement of the steel mesh are illustrated in Figure 2.



Figure 2. Casting mold (internal dimensions: 50 x 50 x 10 cm).

The three different types of prepared specimens are depicted in Figures 3, 4, and 5.



Figure 3. Blast test specimen with PCC content.



Figure 4. Blast test specimen with 5% CFGC content.



Figure 5. Blast test specimen with 10% CFGC content.

To determine the workability of the fresh concrete mixtures, the flow spread diameters of the prepared specimens were measured. The obtained values for each mix design are presented in Table 2.

Table 2. Flow diameters of 50x50x10 cm poured specimens (cm).

Specimens	PCC	5% CFGC	10% CFGC
Average value	10.7	10.1	9.7

During mixing, the ceramic fibers dissolve and form a gel-like structure upon contact with the alkaline liquids, water, and superplasticizer. Consequently, the high-temperature damage caused by an explosion is minimized, as the uniformly distributed fiber gel acts as a protective barrier within the geopolymer matrix (Dağlıç and Yılmaz Polat, 2024). However, because the ceramic fibers absorb some of the mixing liquid, the workability of the fresh concrete is slightly reduced. Therefore, as the ceramic fiber ratio in the specimens increased, the flow spread diameter decreased.

The 15 specimens cast in the laboratory were cured for 28 days and then taken to the blast test site. The 5% CFGC, 10% CFGC, and 50 × 50 × 10 cm PCC slabs were subjected to blast loading using 50, 100, 150, 200, and 250 g of dynamite (trinitroglycerin). The concrete slabs were in direct contact with the explosive during the blast tests. In all blasts, a 5 × 5 × 50 cm wooden formwork frame supported the concrete specimens above the ground. The reason for using the wooden frame was to isolate the concrete from the ground in the event of an explosion. Thus, the energy released during the explosion could not be absorbed by the ground, and the environmental factors and ground-coupling effects during the explosion were largely prevented. Furthermore, the purpose of the wooden frame was to prevent the concrete specimens from being damaged by wood fragmentation under the blast load. In addition, the ambient air temperature during the tests was recorded as 9 °C, wind speed as 4.2 km/h, and humidity as 68%. Due to the destructive nature of the experiments, each configuration was tested once; therefore, statistical error bars such as standard deviation or confidence intervals are not applicable.

Table 3. TNG explosive weights applied to the specimens.

	50 g	100 g	150 g	200 g	250 g
PCC	✓	✓	✓	✓	✓
5% CFGC	✓	✓	✓	✓	✓
10% CFGC	✓	✓	✓	✓	✓

After the blast tests, the specimens were modeled in a computer environment using the ANSYS-Workbench program. In this way, experimental and theoretical data could be compared.

Table 4 presents the studies conducted to determine the trinitrotoluene (TNT) equivalence of the explosive used in the blast tests. The pressure-time data during the blast events were recorded using pressure sensors (Bakır et al., 2024).

Table 4. Sensor placement details (Bakır et al., 2024).

Parameter name	Parameter value
Distance between explosive and sandwich slab (m)	1.85
Explosive weight (kg)	0.91
Sensor height above ground (m)	1.85
Distance between explosive and sensor (m)	3.20

Table 5. Sensor readings (Bakır et al., 2024).

Sensor data	Strenght (N/mm ²)	Time	Z value (m/kg ^{1/3})	W (kg)
Maximum strenght	52924	8.590098	3.866359	0.570274
Minimum strenght	-11795.8	8.594297	3.866359	0.570274

From strength values given in Table 5, the equivalent explosive weight is calculated as $W_{TNT} = 0.57$ kg. The TNT equivalence factor of the TNG type explosive in the contact explosion tests is given in equation (1):

$$\frac{W_{TNT}}{W_{TNG}} = \frac{0.57}{0.91} = 0.62 \quad (1)$$

While modelling, 1 kg TNG was calculated as equivalent to 0.62 g TNT (Bakır et al., 2024). The parameter values used in the program for geopolymer concrete and PCC are given in Table 6.

Table 6. Parameter values used in ANSYS-Workbench modelling.

Specimens	Density (kg/m ³)	Specific heat (J/kg°C)
PCC	2343	654
5% CFGC	2497	830.64
10% CFGC	2497	1007.30

Density values were measured in the laboratory, and the specific heat values were calculated. The specific heat capacity of the ceramic fibers used is 4186.8 J/(kg·°C). Since the ceramic fibers were incorporated by volume, the specific heat of the fiber-reinforced geopolymer concrete was determined using the interpolation method. The concrete models are illustrated in Figures 6–9.

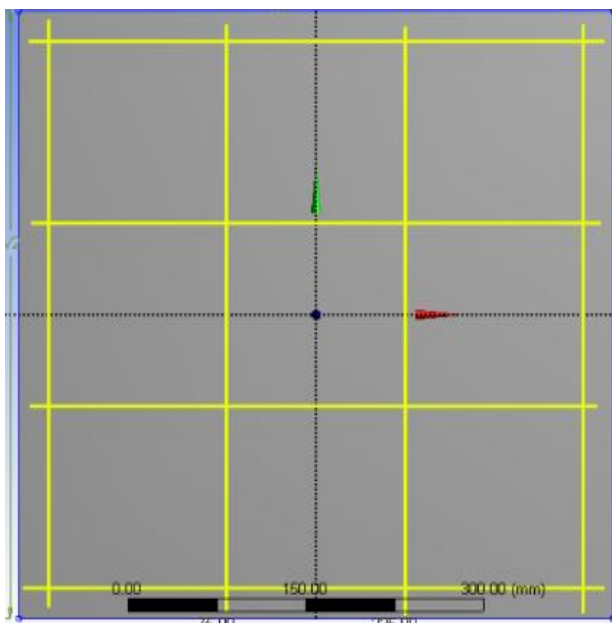


Figure 6. Concrete model and steel mesh top view.

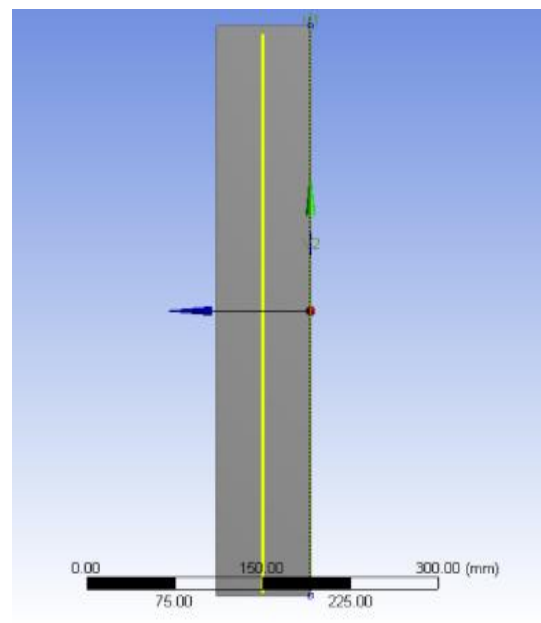


Figure 7. Concrete model and steel mesh side view.

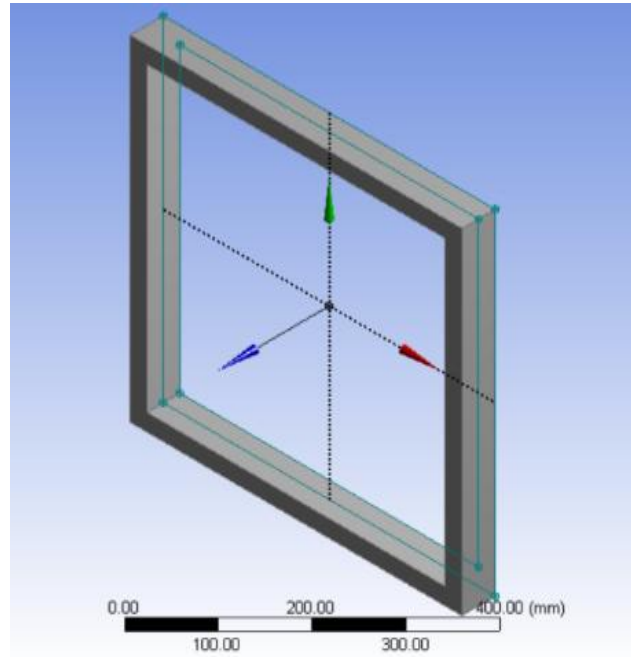


Figure 8. Support modeling.

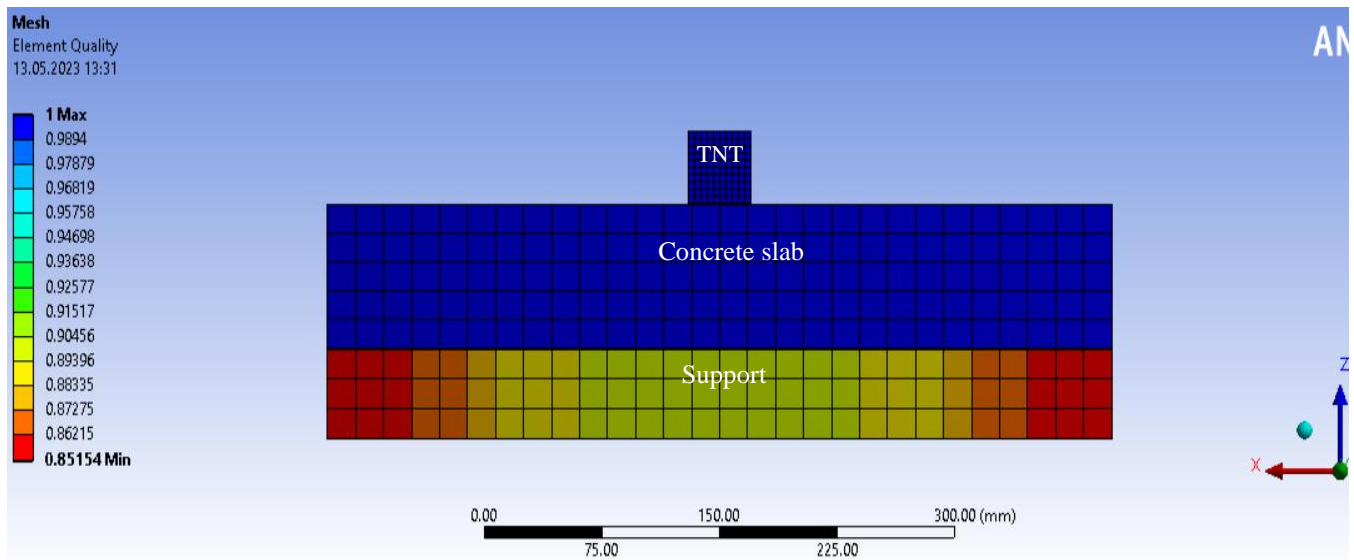


Figure 9. Blast modelling image.

3. Experimental results and analysis

3.1. Explosion tests

Concrete typically loses its structural integrity due to the extreme pressures and high temperatures generated during explosions (Agrawal, 2010; Ngo et al.; Ramsay, 2007; Mortar et al., 2017) This loss of strength significantly exacerbates the overall damage, as the disintegrated concrete fragments and acts as deadly secondary projectiles. This study aims to mitigate such damage by developing a concrete composite capable of better withstanding blast-induced pressures and thermal shocks. To this end, the 15 cast specimens were subjected to blast loading, and their dynamic responses were compared. As illustrated in Figure 10, the specimens were placed on a $5 \times 5 \times 50$ cm wooden frame to isolate them from the ground. This setup prevented the underlying soil from absorbing the blast energy, thereby eliminating ground-coupling effects



Figure 10. The blast mechanism.

Table 7 shows the crater diameter and depth of the specimens due to the explosions.

Table 7. Crater diameters and crater depths formed as a result of explosions (cm).

Crater diameter and depth of specimens (cm)						
Explosive weight	PCC		5% CFGC		10% CFGC	
	Diameter	Depth	Diameter	Depth	Diameter	Depth
50 g	0	0	0	0	0	0
100 g	24	2.0	21	2.5	20	2.5
150 g	33	5.0	31	3.2	28	3.5
200 g	disbanded	disbanded	disbanded	disbanded	34	7.3
250 g	disbanded	disbanded	disbanded	disbanded	disbanded	disbanded

In the tests utilizing 200 g of trinitroglycerin (TNG), only the 10% ceramic fiber-reinforced geopolymer concrete (10% CFGC) slabs remained intact enough for crater diameter and depth measurements. In contrast, during the 250 g TNG experiments, all specimens were extensively damaged, preventing any quantifiable measurement. Figure 11 illustrates the crater diameter damage modes, while Figure 12 depicts the crater depth damage modes resulting from the explosions. Because no significant damage was observed at 50 g TNG, and all specimens were completely fragmented at 250 g TNG, these results

are excluded from Figures 11 and 12. Similarly, since the Portland cement concrete (PCC) and 5% CFGC specimens were fully fragmented at the 200 g TNG level, their values are omitted from these figures.

Crater dimensions were measured using calipers and image-based techniques. Due to the destructive nature of blast testing, each configuration was subjected to a single event; thus, statistical variability (e.g., standard deviation) could not be assessed. Instead, the reported uncertainty corresponds to instrumental measurement error. Based on the resolution and precision of the calipers and imaging tools, the measurement uncertainty was estimated at ± 0.2 mm, representing the limitations of the measurement apparatus rather than experimental reproducibility.

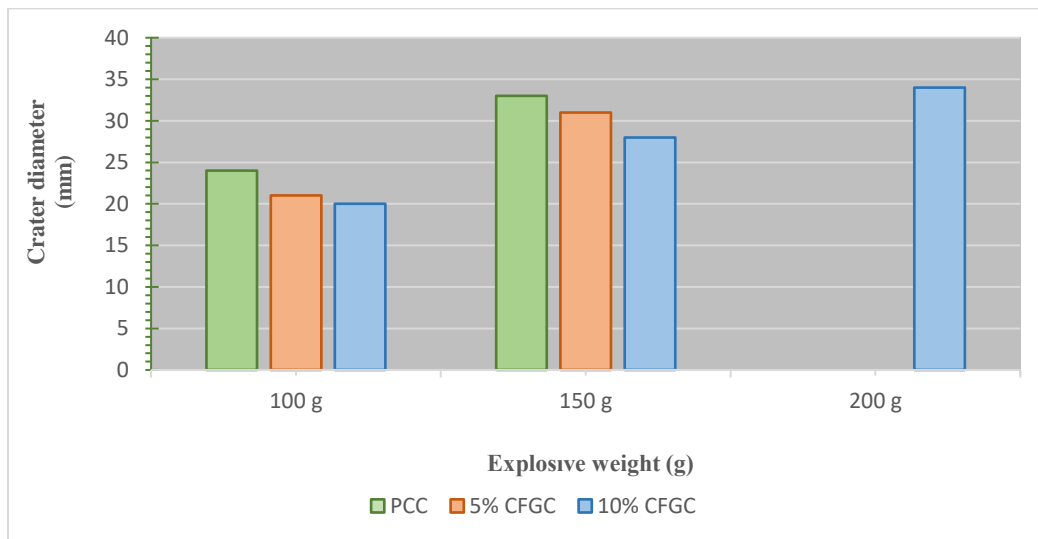


Figure 11. Crater diameter as a function of explosive weight for PCC, 5% CFGC, and 10% CFGC specimens. Each bar represents the crater diameter measured from a single detonation test.

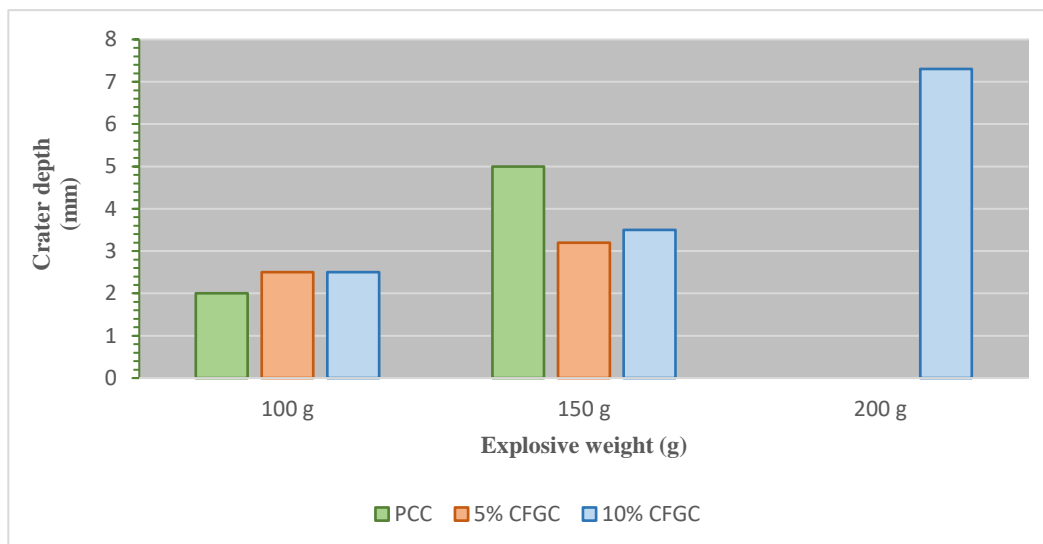


Figure 12. Crater depths as a function of explosive weight for PCC, 5% CFGC, and 10% CFGC specimens. Each bar represents the crater diameter measured from a single detonation test.

Crater diameter and depth damages of 5%, 10% CFGC and PCC slabs detonated with 100 g TNG are shown in Figures 13-18.



Figure 13. The crater diameter of PCC exploded with 100 g TNG.



Figure 14. The crater diameter of 5% CFGC exploded with 100 g TNG.



Figure 15. The crater diameter of 10% CFGC exploded with 100 g TNG.



Figure 16. The crater depth of PCC exploded with 100 g TNG.

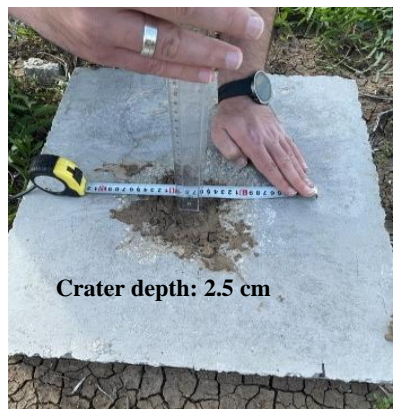


Figure 17. The crater depth of 5% CFGC exploded with 100 g TNG.



Figure 18. The crater depth of 10% CFGC exploded with 100 g TNG.

Among the specimens subjected to the 100 g TNG blast, the 10% CFGC slab exhibited the superior performance with a crater diameter of 20 cm, representing the least damaged specimen. In contrast, the PCC slab sustained the most extensive damage, recording the maximum crater diameter at this charge level. The resulting crater diameter and depth profiles for the 5% CFGC, 10% CFGC, and PCC slabs under 150 g TNG loading are illustrated in Figures 19–24.



Figure 19. The crater diameter of PCC exploded with 150 g TNG.



Figure 20. The crater diameter of 5% CFGC exploded with 150 g TNG.

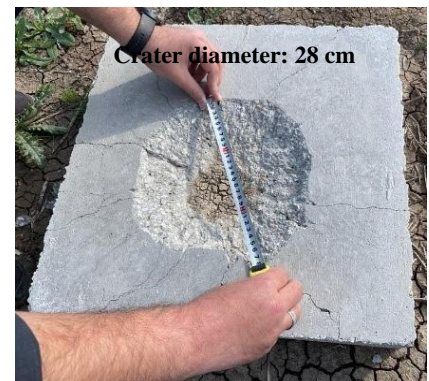


Figure 21. The crater diameter of 10% CFGC exploded with 150 g TNG.



Figure 22. The crater depth of PCC exploded with 150 g TNG.



Figure 23. The crater depth of 5% CFGC exploded with 150 g TNG.

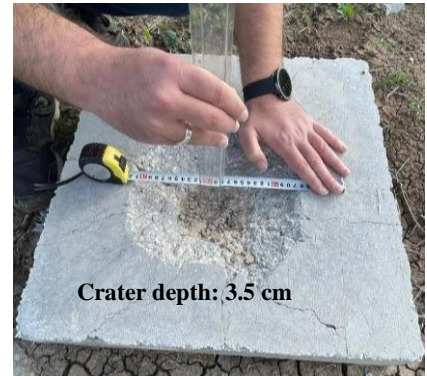


Figure 24. The crater depth of 10% CFGC exploded with 150 g TNG.

The 10% CFGC slab with a crater diameter of 28 cm was the least damaged specimen in the test using 150 g TNG. In the experiment using 150 g of explosive, PCC slab suffered the highest crater diameter damage. The damages of the specimens detonated using 200 g TNG are shown in Figures 25-28.



Figure 25. PCC slab after explosion with 200 g TNG.

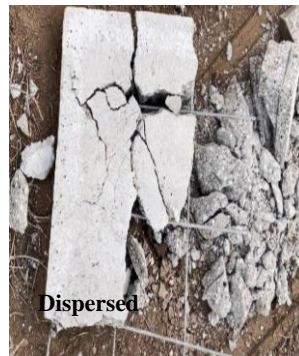


Figure 26. 5% CFGC slab after explosion with 200 g TNG.



Figure 27. 10% CFGC crater diameter after detonation with 200 g TNG.

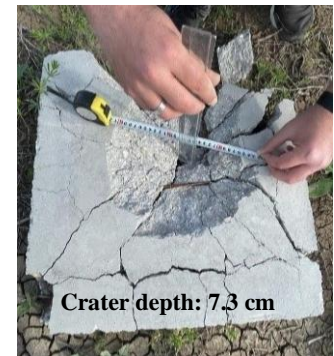


Figure 28. 10% CFGC crater depth after detonation with 200 g TNG.

Among the specimens subjected to the 200 g TNG blast, the 10% CFGC slab exhibited the minimum damage. In contrast, both the 5% CFGC and PCC slabs underwent complete fragmentation, preventing the measurement of crater diameters and depths. However, comparatively, the 5% CFGC slab showed fewer fragments and less disintegration than the PCC specimen. In the 250 g TNG blast tests, crater dimensions could not be quantified as all concrete types were fully fragmented. The post-blast states of the three different concrete types subjected to 250 g TNG are depicted in Figures 29–31.



Figure 29. PCC slab after explosion with 250 g TNG.



Figure 30. 5% CFGC slab after the explosion with 250 g TNG.



Figure 31. 10% CFGC slab after explosion with 250 g TNG.

Among the specimens subjected to 250 g TNG, the 10% CFGC slab exhibited the minimum degree of fragmentation, whereas the most extensive disintegration was observed in the PCC specimen. Throughout the experiments across various explosive charges, the 10% CFGC slabs consistently demonstrated superior resistance to fragmentation compared to the other concrete types. Conversely, the PCC slabs exhibited the highest susceptibility to blast-induced damage. It was observed that the ceramic fibers, having dissolved into a gel-like consistency, functioned as a protective barrier within the geopolymer matrix, thereby mitigating the extreme pressure and thermal effects of the explosions.

While existing literature suggests that steel mesh or steel fibers are typically incorporated to enhance blast resistance by absorbing energy (Foglar et al., 2015; Li et al., 2017; Meng et al., 2020, 2019a), the ceramic fiber utilized in this study offers a distinct mechanism. Unlike conventional reinforcements, these fibers form a homogeneous gel that provides a significant dampening effect and enhances energy dissipation. Consequently, geopolymer concrete slabs reinforced with ceramic fibers sustained markedly less cratering damage (both in diameter and depth) relative to the PCC control. Following the experimental phase, numerical modeling was performed to further validate these findings.

3.2. Modeling

Various software packages can be utilized to perform blast simulations, primarily due to the sudden and highly nonlinear pressure effects inherent in explosive events (Ngo et al., ;Ramsay, 2007). Predicting the rapid and irregular transitions in material behavior under blast loading requires advanced computational tools capable of high-fidelity modeling. This study integrates experimental work with numerical modeling to analyze the response of concrete to blast loads and to provide an engineering approximation of its actual dynamic behavior. The experimental blast tests were simulated using the finite element method (FEM) within the ANSYS Workbench environment. Notably, the tests involving 50 g of explosives were not modeled, as the specimens exhibited no visible damage at this charge level. In Figures 32-34, the blast tests using 100 g TNG were modeled using the finite element method.

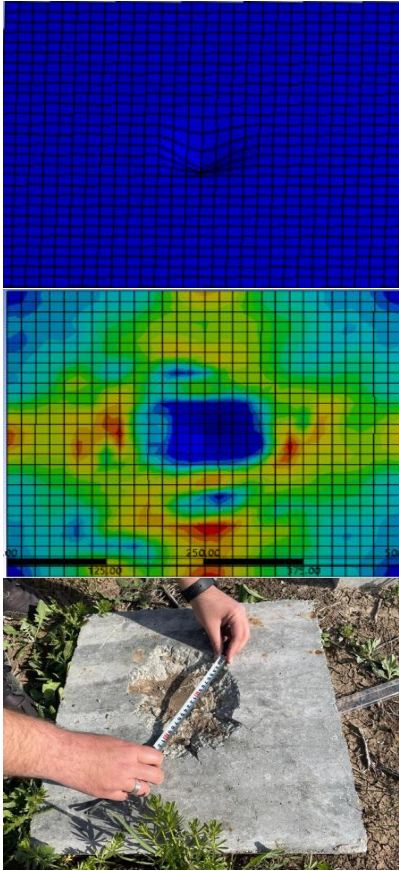


Figure 32. Modelling of PCC slab detonated with 100 g TNG in ANSYS-Workbench.

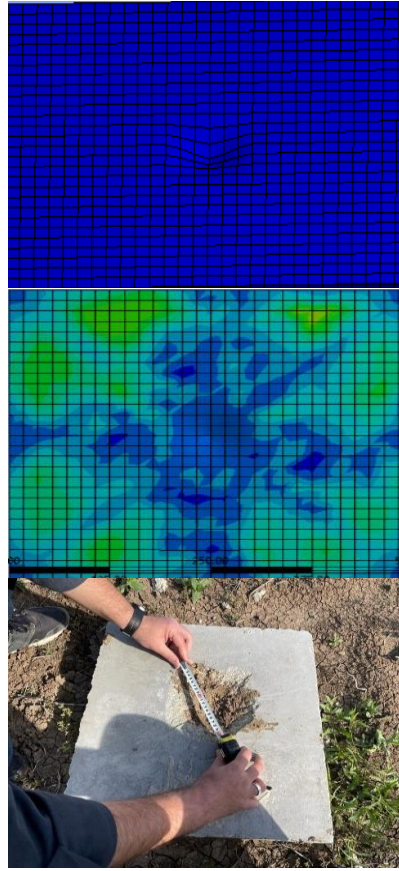


Figure 33. Modelling of 5% CFGC slab detonated with 100 g TNG in ANSYS-Workbench.

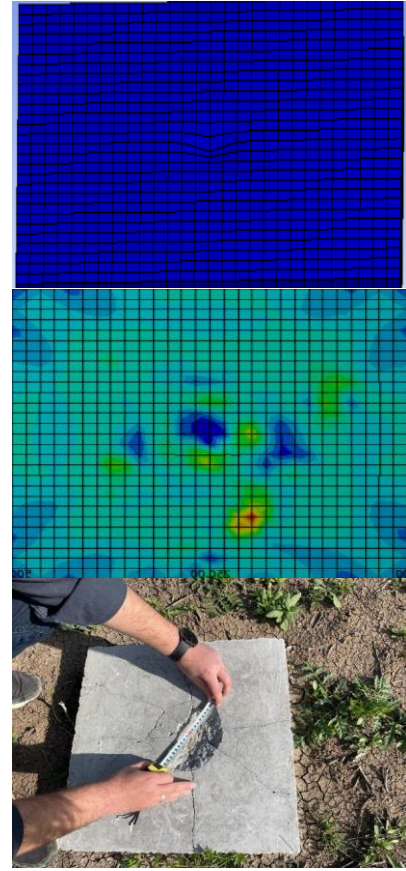


Figure 34. Modelling of 10% CFGC slab detonated with 100 g TNG in ANSYS-Workbench.

In Figures 35-37, the blast test using 150 g TNG was modelled using the finite element method.

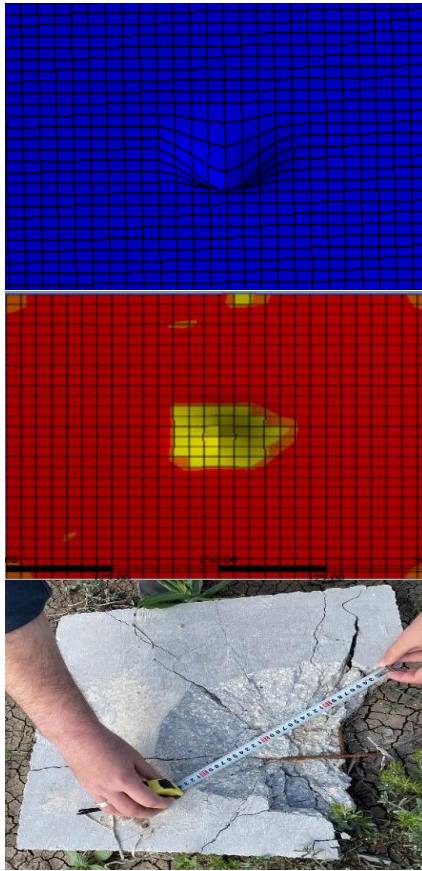


Figure 35. Modelling of PCC slab detonated with 150 g TNG in ANSYS-Workbench.

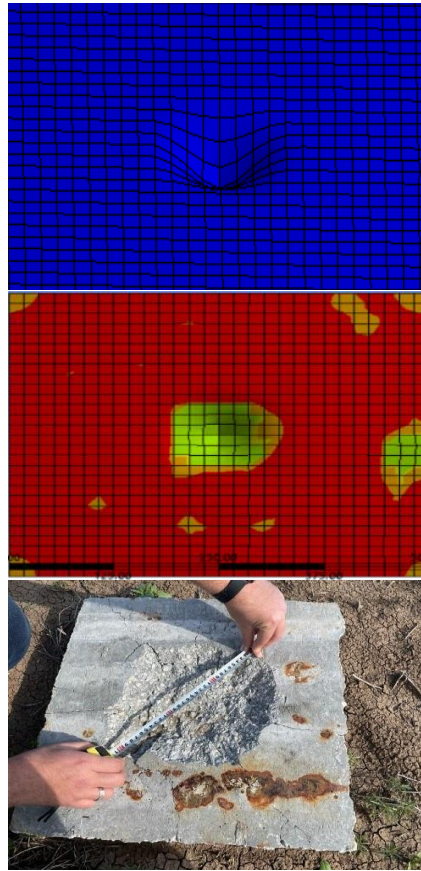


Figure 36. Modelling of 5% CFGC slab detonated with 150 g TNG in ANSYS-Workbench.

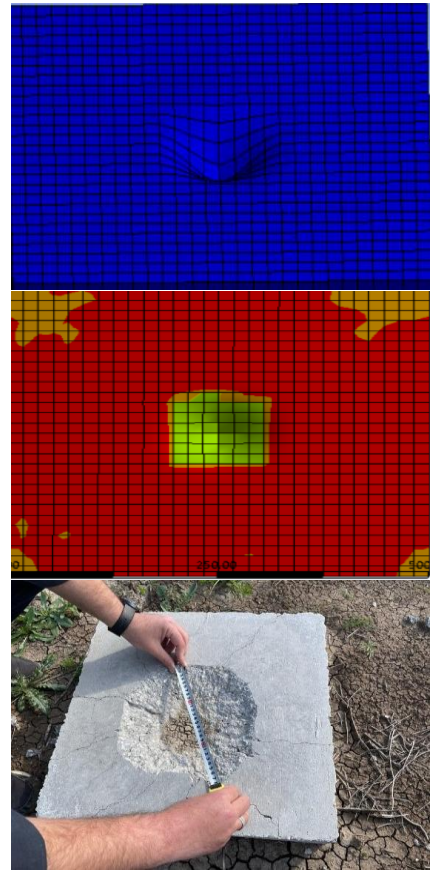


Figure 37. Modelling of 10% CFGC slab detonated with 150 g TNG in ANSYS-Workbench.

Figure 38 shows the modelling of the 10% CFGC slab, which did not disintegrate and remained as a single piece among the specimens tested with 200 g TNG.

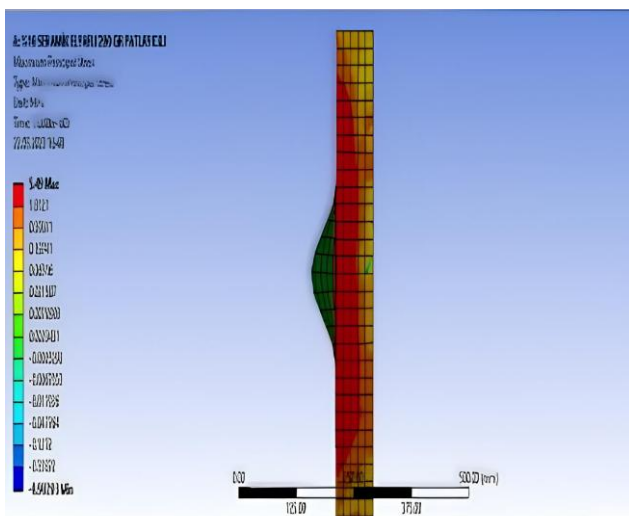


Figure 38. Modelling of 10% CFGC slab detonated with 200 g TNG in ANSYS-Workbench.



Figure 39. 10% CFGC slab after explosion with 200 g TNG.

Figures 40, 41 and 42 show the models of the specimens under the effect of 250 g TNG.

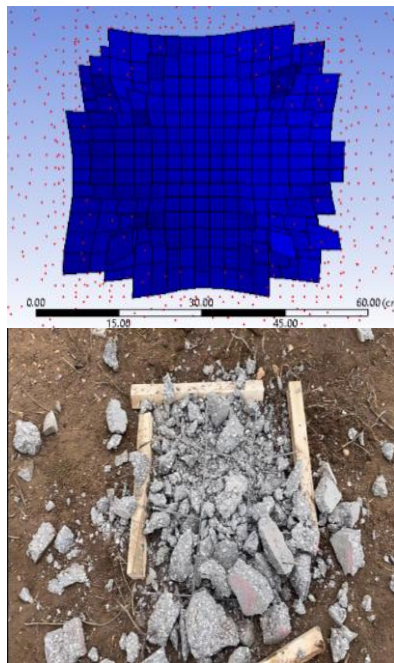


Figure 40. Modelling of PCC slab detonated with 250 g TNG in ANSYS-Workbench.

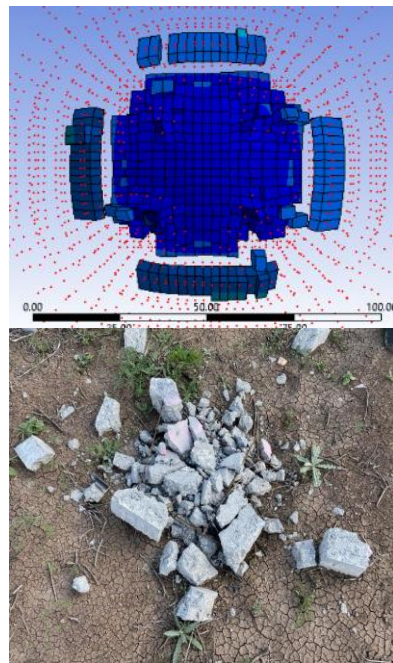


Figure 41. Modelling of 5% CFGC slab detonated with 250 g TNG in ANSYS-Workbench.

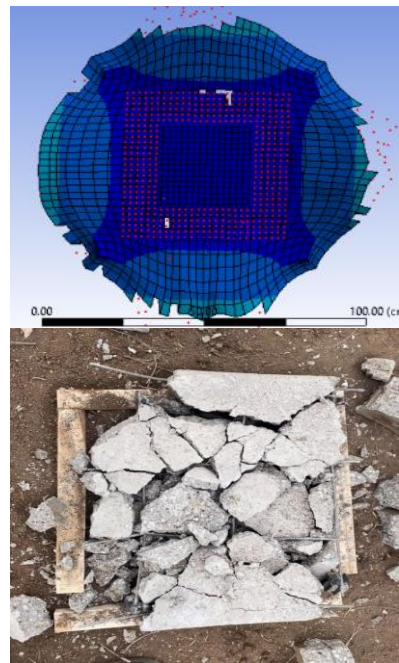


Figure 42. Modelling of 10% CFGC slab detonated with 250 g TNG in ANSYS-Workbench.

All specimens subjected to 250 g TNG blasts underwent complete fragmentation and sustained severe structural deformation. The numerical simulations for the 250 g TNG charge yielded fragmentation patterns that closely correlated with the experimental observations. The deformation damage across both geopolymer and PCC slabs modeled in ANSYS Workbench was consistent with the damage modes recorded during the experimental blasts. In simulations utilizing 100, 150, 200, and 250 g TNG, the 10% CFGC slab exhibited the minimum damage, whereas the PCC slab sustained the most extensive failure, mirroring the experimental results.

This strong correlation suggests that the response of CFGC to blast loading can be accurately predicted by adjusting specific parameters within the numerical model, providing a reliable tool for future structural assessments. Overall, the 10% CFGC slab, characterized by the highest ceramic fiber content, consistently demonstrated the superior resistance to fragmentation. Conversely, the PCC specimens without fiber reinforcement exhibited the highest susceptibility to blast-induced disintegration. These findings confirm that increasing the ceramic fiber content in geopolymer concrete significantly enhances its blast resistance.

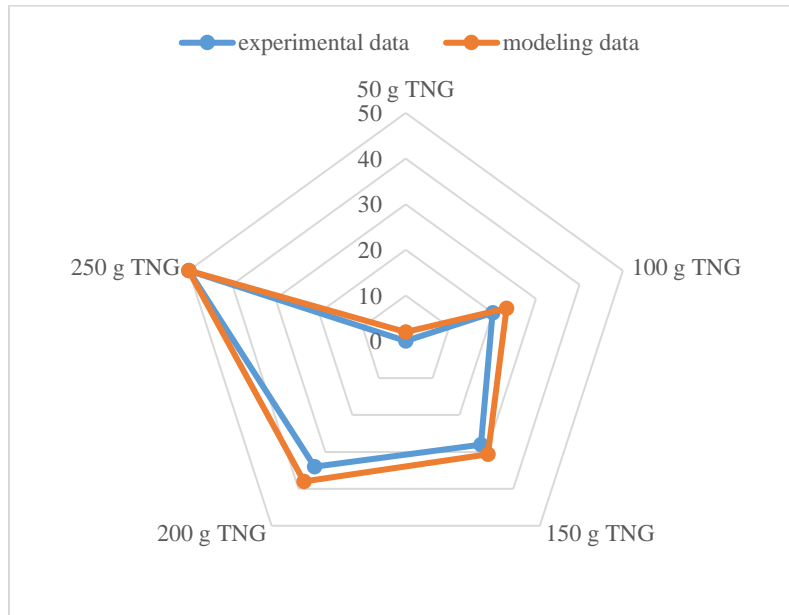


Figure 43. Comparison of experimental and modeling data of 10% CFGC specimen under explosions.

- A comparison between the experimental and ANSYS Workbench modeling results revealed an average error rate of 7.5%.
- A strong correlation was observed between the small-scale blast tests and the numerical simulations regarding crater diameter and depth.
- While the numerical models closely aligned with the experimental data, certain discrepancies were noted under high blast loads (200 g TNG and above).
- These variances can be attributed to material heterogeneity, inherent modeling assumptions, and the complex fluctuations in explosion dynamics.

In summary, it is evident that blast-induced damage decreases as the ceramic fiber content in geopolymer concrete increases. By investigating the blast response of ceramic fiber-reinforced geopolymer concrete (CFGC), this study contributes significant findings to the literature, demonstrating that CFGC structures exhibit superior resistance to high-pressure and high-temperature waves compared to plain concrete structures. The findings suggest that incorporating ceramic fibers into high-strength concrete for military facilities, critical infrastructure, and civil buildings in high-risk areas can substantially mitigate blast-induced damage. Nonetheless, further extensive research is required to optimize these structural results

4. Conclusions and comments

In this study, the response of ceramic fiber-reinforced geopolymer concrete (CFGC) to blast loading was investigated through both experimental and numerical approaches. The key findings are summarized as follows:

1. Under 100 g trinitroglycerin (TNG) blast loading, the crater diameter of the PCC slab was 14.29% and 20.00% greater than those of the 5% CFGC and 10% CFGC slabs, respectively.
2. For 150 g TNG blasts, the crater diameter damage in the PCC slab was 6.45% and 17.86% higher compared to the 5% CFGC and 10% CFGC specimens, respectively.
3. While the PCC slab was completely fragmented under a 200 g TNG blast, the 10% CFGC slab exhibited the highest resistance with minimal disintegration, demonstrating the superior energy dissipation of the ceramic fiber gel matrix.
4. CFGC specimens (5% and 10%) showed significantly reduced spalling and a mitigated shrapnel effect compared to the PCC control under 200 g TNG loading.

5. At the maximum charge of 250 g TNG, all specimens underwent fragmentation; however, the 10% CFGC slab consistently showed the least extensive damage, whereas the PCC slab sustained total destruction.
6. The results indicate a positive correlation between ceramic fiber content and the homogeneous damping of blast energy within the geopolymer matrix.
7. The numerical data obtained via ANSYS Workbench were highly consistent with the experimental blast test results, validating the predictive accuracy of the finite element model.

Overall, the incorporation of ceramic fibers into geopolymer concrete significantly enhances its resistance to high-pressure and high-temperature waves. While CFGC effectively mitigates damage at low-to-moderate blast levels, extreme energy levels still lead to structural failure, necessitating further optimization.

To build upon the findings of this study, the following directions are suggested:

- The influence of structural parameters, such as gradually increasing slab thickness or reinforcement ratios, should be investigated to identify ultimate failure thresholds.
- Comparative studies could be conducted on specimens with varying compressive strengths to isolate the effects of matrix toughness versus matrix strength.
- Future experimental setups should incorporate high-speed instrumentation, such as LVDTs and accelerometers, to generate larger datasets for deep learning-based predictive models and advanced multi-physics simulations.
- Given that the ceramic fibers in this study were integrated in a dissolved gel form, future research should explore the hybrid effects of combining ceramic fiber gel with discrete steel fibers to optimize both energy absorption and tensile ductility under blast loading.

Author contributions: Aras Dalğıç: Experimental study execution, finite element method analysis, explosion field studies, article writing, results and recommendations. Berivan Yılmazzer Polat: Research design methodology, experimental study, conceptualization, article writing, results and recommendations. Sedat Savaş: Explosion field studies.

Funding: This study was supported by the Scientific and Technical Research Council of Turkey (TÜBİTAK) under project number 221M204.

Acknowledgments: Assist. Dr. Sedat Savaş is included in this article because he was a member of this research project and was responsible for the explosion testing of this article. The authors would also like to thank Dr. Dursun Bakır for his support.

Conflicts of interest: The authors declare that there are no conflicts of interest regarding this research work.

References

- Agrawal, J. P. (2010). High Energy Materials: Propellants, Explosives and Pyrotechnics. In *High Energy Materials: Propellants, Explosives and Pyrotechnics*. <https://doi.org/10.1002/9783527628803>
- Bakır, D., Savaş, S., and Üstündağ, H. (2024). Simulation of the behavior of reinforced concrete rectangular hollow sandwich plates under the effect of contact explosion through SPH method. *Revista de La Construcción*, 23(3), 554–567. <https://doi.org/10.7764/RDLC.23.3.554>
- Dalğıç, A., and Yılmazzer Polat, B. (2024). The Behavior of Ceramic Fiber Geopolymer Concrete under the Effect of High Temperature. *Applied Sciences (Switzerland)*, 14(4), 1607. <https://doi.org/10.3390/app14041607>
- Duc Ngo, Tuan; Mendis, P.; Gupta, A.; Ramsay, J. (2007). Blast loading and blast effects on structures-an overview. *EJSE Special Issue: Loading on Structures*, 7, 76–91. Retrieved from <https://www.researchgate.net/publication/270162972>
- Foglar, M., Hajek, R., Kovar, M., and Štoller, J. (2015). Blast performance of RC panels with waste steel fibers. *Construction and Building Materials*, 94, 536–546. <https://doi.org/10.1016/j.conbuildmat.2015.07.082>
- Hardjito, D., and Rangan, B. V. (2005). Development and properties of low-calcium fly ash-based geopolymer concrete. *Research Report GC*, 94. Retrieved from http://www.geopolymer.org/fichiers_pdf/curtin-flyash-GP-concrete-report.pdf

- Ibrahim Haruna, S., Zhu, H., Jiang, W., and Shao, J. (2021). Evaluation of impact resistance properties of polyurethane-based polymer concrete for the repair of runway subjected to repeated drop-weight impact test. *Construction and Building Materials*, 309, 125152. <https://doi.org/10.1016/j.conbuildmat.2021.125152>
- Li, J., Wu, C., Hao, H., and Su, Y. (2017). Experimental and numerical study on steel wire mesh reinforced concrete slab under contact explosion. *Materials and Design*, 116, 77–91. <https://doi.org/10.1016/j.matdes.2016.11.098>
- Ma, Y., Zhu, B., and Tan, M. (2005a). Properties of ceramic fiber reinforced cement composites. *Cement and Concrete Research*, 35(2), 296–300. <https://doi.org/10.1016/j.cemconres.2004.05.017>
- Ma, Y., Zhu, B., and Tan, M. (2005b). Properties of ceramic fiber reinforced cement composites. *Cement and Concrete Research*, 35(2), 296–300. <https://doi.org/10.1016/j.cemconres.2004.05.017>
- McCaffrey. (2002). *GCL: Environmental special issue 2002 climate change and the cement industry*. 15–19.
- Meng, Q., Wu, C., Hao, H., Li, J., Wu, P., Yang, Y., and Wang, Z. (2020). Steel fibre reinforced alkali-activated geopolymer concrete slabs subjected to natural gas explosion in buried utility tunnel. *Construction and Building Materials*, 246, 118447. <https://doi.org/10.1016/j.conbuildmat.2020.118447>
- Meng, Q., Wu, C., Su, Y., Li, J., Liu, J., and Pang, J. (2019a). A study of steel wire mesh reinforced high performance geopolymer concrete slabs under blast loading. *Journal of Cleaner Production*, 210, 1150–1163. <https://doi.org/10.1016/j.jclepro.2018.11.083>
- Meng, Q., Wu, C., Su, Y., Li, J., Liu, J., and Pang, J. (2019b). Experimental and numerical investigation of blast resistant capacity of high performance geopolymer concrete panels. *Composites Part B: Engineering*, 171(September 2018), 9–19. <https://doi.org/10.1016/j.compositesb.2019.04.010>
- Mortar, N. A. M., Hussin, K., Razak, R. A., Abdullah, M. M. A. B., Hilmi, A. H., and Sandu, A. V. (2017). Properties and Behavior of Geopolymer Concrete Subjected to Explosive Air Blast Loading: A Review. *MATEC Web of Conferences*, 97. <https://doi.org/10.1051/mateconf/20179701019>
- Naik, T. R. (2008). Sustainability of Concrete Construction. *Practice Periodical on Structural Design and Construction*, 13(2), 98–103. [https://doi.org/10.1061/\(asce\)1084-0680\(2008\)13:2\(98\)](https://doi.org/10.1061/(asce)1084-0680(2008)13:2(98))
- Nili, M., and Afrouhsabet, V. (2010). Combined effect of silica fume and steel fibers on the impact resistance and mechanical properties of concrete. *International Journal of Impact Engineering*, 37(8), 879–886. <https://doi.org/10.1016/j.ijimpeng.2010.03.004>
- Polat, B. Y., Savaş, S., and Polat, A. (2023). Anti-tank impact absorption with a reinforced concrete plate design. *Advances in Concrete Construction*, 15(4), 229–239. <https://doi.org/10.12989/acc.2023.15.4.229>
- Shi, Y., Wang, J., and Cui, J. (2020). Experimental studies on fragments of reinforced concrete slabs under close-in explosions. *International Journal of Impact Engineering*, 144, 103630. <https://doi.org/10.1016/j.ijimpeng.2020.103630>
- Su, H., Xu, J., and Ren, W. (2014). Mechanical properties of ceramic fiber-reinforced concrete under quasi-static and dynamic compression. *Materials and Design*, 57, 426–434. <https://doi.org/10.1016/j.matdes.2013.12.061>
- V. M. Malhotra. (2002). Introduction: Sustainable Development and Concrete Technology. *Concrete International*, 24(7), 22.
- Vora, P. R., and Dave, U. V. (2013). Parametric studies on compressive strength of geopolymer concrete. *Procedia Engineering*, 51, 210–219. Elsevier Ltd. <https://doi.org/10.1016/j.proeng.2013.01.030>
- Wu, J., Zhou, Y., Zhang, R., Liu, C., and Zhang, Z. (2020). Numerical simulation of reinforced concrete slab subjected to blast loading and the structural damage assessment. *Engineering Failure Analysis*, 118(August), 104926. <https://doi.org/10.1016/j.engfailanal.2020.104926>
- Yazici, Ş., Arel, H. Ş., and Tabak, V. (2013, April 1). The effects of impact loading on the mechanical properties of the SFRCs. *Construction and Building Materials*, Vol. 41, pp. 68–72. Elsevier. <https://doi.org/10.1016/j.conbuildmat.2012.11.095>



Copyright (c) 2026 Dalğıç, A., Yılmazzer Polat, B. and Savaş, S. This work is licensed under a [Creative Commons Attribution-NonCommercial-No Derivatives 4.0 International License](https://creativecommons.org/licenses/by-nc-nd/4.0/).